Supplmentary Material
Quantum-limited time-frequency estimation through mode-selective photon measurement

J. M. Donohue,[1,*] V. Ansari,[1] J. Řeháček,[2] Z. Hradil,[2] B. Stoklasa,[2] M. Paúr,[2] L. L. Sánchez-Soto,[3,4] and C. Silberhorn[1]

[1]*Integrated Quantum Optics, Paderborn University, Warburger Strasse 100, 33098 Paderborn, Germany*
[2]*Department of Optics, Palacký University, 17. listopadu 12, 771 46 Olomouc, Czech Republic*
[3]*Departamento de Óptica, Facultad de Física, Universidad Complutense, 28040 Madrid, Spain*
[4]*Max-Planck-Institute für die Physik des Lichts, Staudtstrasse 2, 91058 Erlangen, Germany*

In this supplementary material, we detail the sum-frequency generation process used to estimate time-frequency separations, including the limitations of the device. We also detail the measurement tomography used to calibrate our technique.

Estimating separations with a quantum pulse gate

In this section, we derive Eq. (6) of the main text, which provides the separation estimators $\hat{\tilde{s}}_\nu$ and $\hat{\tilde{s}}_t$ for measurements made with a quantum pulse gate (QPG). The quantum pulse gate operation relies on a large discrepancy between the group velocities of the input and upconverted signals, which manifests in the energy picture as a much larger input acceptance bandwidth than output signal bandwidth. In practice, this discrepancy is of course finite, which places limitations on the achievable time and frequency resolutions. Here, starting from the basic nonlinear interaction, we outline these limitations.

In our treatment herein, we assume that the three-field interaction takes place inside a single-mode $\chi^{(2)}$ waveguide, such that we may neglect the spatial modes involved. We also assume that we are working in the low-efficiency regime, such that a first-order approach is sufficient [45, 47]. We label the modes as the input ("1"), the QPG pump ("2"), and upconverted output ("3"), and group the central frequencies into the variables as $\tilde{\nu} = \nu - \nu_0$. In this case, the upconverted spectral amplitude $\gamma(\tilde{\nu}_3)$ is related to the spectral amplitude of the QPG pump $\alpha(\tilde{\nu}_2)$ and the input signal $\psi(\tilde{\nu}_1)$ as

$$\gamma(\tilde{\nu}_3) = \theta \int \mathrm{d}\tilde{\nu}_1 H(\tilde{\nu}_1, \tilde{\nu}_3)\alpha(\tilde{\nu}_3 - \tilde{\nu}_1)\psi(\tilde{\nu}_1), \tag{1}$$

where energy conservation $\tilde{\nu}_2 = \tilde{\nu}_3 - \tilde{\nu}_1$ has been accounted for, θ is a coupling constant representing factors such as the material nonlinearity, and $H(\tilde{\nu}_1, \tilde{\nu}_3)$ is the phasematching function, characterized by the relationships between the wavenumbers $k_j(\tilde{\nu}_j) = \frac{2\pi\nu_j n_j(\tilde{\nu}_j)}{c}$ of the interacting fields.

If process is phasematched at the central frequencies through periodic poling and chromatic dispersion within each field can be neglected, the phasematching function for an interaction length L can be expressed as

$$H(\tilde{\nu}_1, \tilde{\nu}_3) \propto L\,\mathrm{sinc}\left(\frac{L[(k_1' - k_2')\tilde{\nu}_1 - (k_3' - k_2')\tilde{\nu}_3]}{2}\right) \tag{2}$$

where $k_j' = \frac{\partial k_j}{\partial \nu_j}\big|_{\nu_{0,j}} = \frac{1}{2\pi u_j}$ is inversely proportional to the group velocity u_j. If the input signal and QPG pump are group-velocity matched $k_1' = k_2'$, the phasematching function simplifies to a function of only the output frequency $\tilde{\nu}_3$. If we use a bandpass filter to remove the side lobes of the sinc function, we can approximate the phasematching function as a Gaussian,

$$H(\tilde{\nu}_3) \approx L e^{-\eta \frac{(L(k_3' - k_1')\tilde{\nu}_3)^2}{4}} := L e^{-\frac{\tilde{\nu}_3^2}{4\sigma_{\mathrm{PM}}^2}}, \tag{3}$$

where σ_{PM} is the RMS phasematching bandwidth and $\eta \approx 0.193$.

We assume that the input signal wavefunction is a Gaussian pulse with some offset $\delta\nu$ from the perfectly phasematched frequencies and a small time delay δt relative to the QPG pump pulse, which we express as

$$\psi(\tilde{\nu}_1) = \frac{1}{(2\pi\sigma_{\tilde{\nu}}^2)^{\frac{1}{4}}} \exp\left[-\frac{(\tilde{\nu} + \delta\nu)^2}{4\sigma_{\tilde{\nu}}^2} - i2\pi\tilde{\nu}\delta t\right]. \tag{4}$$

Note that the RMS width of the pulse in time is $\sigma_t = 1/(4\pi\sigma_\nu)$. The QPG pump pulse is shaped to the first two Hermite-Gauss temporal modes with bandwidth σ_2, given by

$$\begin{aligned} \alpha_{\wedge}(\tilde{\nu}_2) &= \frac{1}{(2\pi\sigma_2^2)^{\frac{1}{4}}} \exp\left[-\frac{\tilde{\nu}_2^2}{4\sigma_2^2}\right] \\ \alpha_{\curlywedge}(\tilde{\nu}_2) &= \frac{\tilde{\nu}_2}{(2\pi\sigma_2^6)^{\frac{1}{4}}} \exp\left[-\frac{\tilde{\nu}_2^2}{4\sigma_2^2}\right]. \end{aligned} \tag{5}$$

Substituting these and the phasematching function into Eq. (1) and finding the relative upconversion probability as $P = \int \mathrm{d}\nu_3 |\gamma(\tilde{\nu}_3)|^2$, the ratio of the upconversion probabilities for the first two modes is found to be

$$\begin{aligned} \frac{P_{\curlywedge}}{P_{\wedge}} &= \sigma_2^2 \left[\frac{\sigma_{\tilde{\nu}}^2 + 16\pi^2\delta t^2\sigma_{\tilde{\nu}}^2\sigma_2^2 + \sigma_2^2}{(\sigma_{\tilde{\nu}}^2 + \sigma_2^2)^2} + \frac{\delta\nu^2 - \sigma_{\tilde{\nu}}^2 - \sigma_2^2 - \sigma_{\mathrm{PM}}^2}{(\sigma_{\tilde{\nu}}^2 + \sigma_2^2 + \sigma_{\mathrm{PM}}^2)^2}\right] \\ &\overset{\sigma_2 = \sigma_{\tilde{\nu}}}{=} \frac{\sigma_{\mathrm{PM}}^2}{2(2\sigma_{\tilde{\nu}}^2 + \sigma_{\mathrm{PM}}^2)} + 4\pi^2\delta t^2\sigma_{\tilde{\nu}}^2 + \frac{\delta\nu^2\sigma_{\tilde{\nu}}^2}{2(2\sigma_{\tilde{\nu}}^2 + \sigma_{\mathrm{PM}}^2)^2} \\ &\overset{\sigma_{\tilde{\nu}}^2 \gg \sigma_{\mathrm{PM}}^2}{\approx} \frac{\sigma_{\mathrm{PM}}^2}{4\sigma_{\tilde{\nu}}^2} + \frac{\delta t^2}{4\sigma_t^2} + \frac{\delta\nu^2}{4\sigma_{\tilde{\nu}}^2}. \end{aligned} \tag{6}$$

To get from the first line to the second, we have set the bandwidth of the QPG pump to be equal to the input signal, ensuring that the two pulses have matched temporal-mode bases. To get from the second line to the third, we have assumed that the phasematching bandwidth is narrower than the input pulses, such that $2\sigma_{\tilde{\nu}}^2 + \sigma_{\mathrm{PM}}^2 \approx 2\sigma_{\tilde{\nu}}^2$. Since $P_{\wedge}$ and $P_{\curlywedge}$ are both symmetric functions of $\delta\nu$ or δt, Eq. (6) holds for incoherent mixtures of positive and negative shifts, and Eq. (6) of

the main text can be retrieved by substituting $\delta\nu \mapsto \frac{\bar{\mathfrak{s}}_\nu}{2}$ and $\delta t \mapsto \frac{\bar{\mathfrak{s}}_t}{2}$. It is apparent that the minimum resolvable shift will be on the order of σ_{PM} in frequency and $\frac{\sigma_{\mathrm{PM}}}{\sigma_\nu}\sigma_t$ in time, and that any misalignment in frequency or time will adversely effect the resolution of measurements in the other setting.

Cramér-Rao bound for the quantum pulse gate

For a perfectly mode-selective device and an infinite number of projections, the Cramér-Rao lower bound (CRLB) on the estimation precision coincides with the quantum bound. As shown in the previous section, the mode-selective properties of the QPG break down for frequency shifts smaller than the phasematching bandwidth, σ_{PM}. Additionally, in the simplified analysis above, we project only onto the first two Hermite-Gauss modes, and the data analysis performed only considers the first three. Here, we consider the CRLB for the measurement scheme we employ, including the effect of limited selectivity and finite mode projections.

We consider access to a finite number of mode projections, ranging from 0 to M and corresponding to the 0th to Mth Hermite-Gaussian time-frequency modes. The probability of photon upconversion when projecting on the jth mode as a function of time or frequency separation $\bar{\mathfrak{s}}$ is given by $P_j(\bar{\mathfrak{s}}) = \int \mathrm{d}\nu_3\, |\gamma(\tilde{\nu}_3, \bar{\mathfrak{s}})|^2$. In our numerical analysis, the normalization is set such that $\lim_{\sigma_{\mathrm{PM}}\to 0} P_0(0) = 1$, effectively normalizing out any external losses but accounting for lost information due to the imperfect selectivity. The Fisher information available in this set of projections for N detected photons can be found in analogy to Eq. (3) of the main text as

$$\mathscr{F}_{\mathrm{QPG}} = N \sum_{j=0}^{M} \frac{1}{P_j(\bar{\mathfrak{s}})} \left[\frac{\partial P_j(\bar{\mathfrak{s}})}{\partial \bar{\mathfrak{s}}}\right]^2. \tag{7}$$

The CRLB for the QPG, found as $1/\mathscr{F}_{\mathrm{QPG}}$, is shown in Fig. 1 for two different nonlinear interaction lengths (and correspondingly two different phasematching bandwidths) and for projections onto two, three, or four Hermite-Gaussian modes. Even when only projecting on the first two Hermite-Gauss modes, there is a large span of separations when the QPG has a strong advantage over standard intensity detection. For large separations, higher-order projections become necessary, but in this limit, standard intensity detection approaches the quantum limit anyhow. For very small separations, $\bar{\mathfrak{s}} \sim \sigma_{\mathrm{PM}}$, the CRLB diverges. The point at which this "curse" kicks in is not set by the point-spread function of the optical signals, as it is for standard intensity detection, but rather the phasematching bandwidth. By increasing the length of the medium, as seen in Fig. 1(b), the scale of the divergence can dramatically improve.

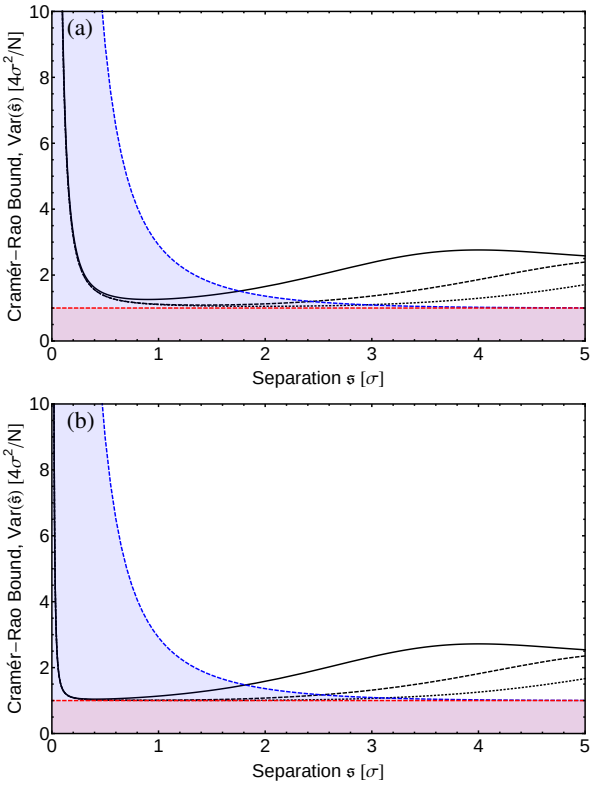

FIG. 1. **Cramér-Rao lower bound for quantum pulse gate measurements.** The Cramér-Rao lower bound on the variance of the estimated time or frequency shift $\bar{\mathfrak{s}}$ is shown using standard intensity detection in blue and by projecting onto the first two, three, or four Hermite-Gauss modes in black (solid, dashed, and dotted line, respectively). The constant quantum limit is shown in red. Plot (a) corresponds to the experimental parameters used, including a 17-mm upconversion medium, while plot (b) corresponds to an upconversion medium five times longer (85 mm).

Measurement tomography methods

In this section, we describe the measurement tomography method used to retrieve an accurate separation estimator from the directly measured data. To characterize the device, we implement projections onto the first three Hermite-Gauss modes, where "ideal measurement" can be described by projections of the input signal on the three lowest-order Hermite-Gauss modes HG_0, HG_1, and HG_2. We denote $q_j(\bar{\mathfrak{s}})$ the probability of the jth measurement output given the true separation is $\bar{\mathfrak{s}}$. For a Gaussian point-spread function (PSF) of width σ, this probability reads

$$q_j(\bar{\mathfrak{s}}) = \frac{1}{j!}\left(\frac{\bar{\mathfrak{s}}}{4\sigma}\right)^{2j} e^{-\left(\frac{\bar{\mathfrak{s}}}{4\sigma}\right)^2}, \qquad j = 0,1,2. \tag{8}$$

Due to unavoidable imperfections, the actual detection probabilities $p_j(\bar{\mathfrak{s}})$ differ slightly from $q_j(\bar{\mathfrak{s}})$ and the measurement device needs to be characterized before using. Assuming the setup works well, that is, the differences between the actual

and target distributions $p_j(\mathfrak{s})$ and $q_j(\mathfrak{s})$ are small, we expand the former using the latter as a basis as follows

$$p_j(\mathfrak{s}) = \sum_{k=0}^{M} c_{jk}\, q_k(\mathfrak{s}), \qquad j = 0,1,2\,. \tag{9}$$

Having repeatedly measured a set of known separations $\mathfrak{s} = \{\mathfrak{s}_1, \mathfrak{s}_2, \ldots, \mathfrak{s}_N\}$, the probabilities p_j can be estimated by the corresponding relative frequencies $f_j = \langle n_j\rangle / \sum_j \langle n_j\rangle$. Denoting further $f_\alpha^j = f_j(\mathfrak{s}_\alpha)$, $q_{k\alpha} = q_k(\mathfrak{s}_\alpha)$, and $c_k^j = c_{jk}$, we obtain three sets of linear equations to be solved for the set of unknown detection coefficients c_k^j

$$f_k^j = \sum_k q_{k\alpha} c_k^j, \qquad j = 0,1,2\,. \tag{10}$$

The pseudo-inverse can be used to obtain standard solutions minimizing the L_2 norm,

$$\mathbf{c}^j = Q^{+}\mathbf{f}^j, \qquad j = 0,1,2\,. \tag{11}$$

It turns out just a few ($M \approx 4$) basis functions in Eq. (8) are required to observe excellent fits of the detected relative frequencies f_j in terms of the corresponding theoretical models p_j for all measured separations in the region of interest $\mathfrak{s} \in [0,2]$.

We next proceed to the parameter estimation step using our characterized measurement. Each measurement returns a three numbers, n_0, n_1, and n_2. Assuming Poissonian statistics, the separation is estimated by maximizing the log-likelihood

$$\hat{\mathfrak{s}} = \arg\max_{\mathfrak{s}} \left\{ \sum_j n_j \log\left[\frac{p_j(\mathfrak{s})}{\sum_{j'} p_{j'}(\mathfrak{s})} \right] \right\} \tag{12}$$

subject to $\hat{\mathfrak{s}} \geq 0$ using a suitable optimization tool. Finally, for every true separation we calculate the statistics of the estimates and compare the measurement errors to the relevant classical and quantum resolution limits.

* john.matthew.donohue@uni-paderborn.de

[1] H. Cramér, *Mathematical Methods of Statistics* (Princeton University Press, Princeton, NJ, 1946).
[2] R. C. Rao, Bull. Calcutta Math. Soc. **37**, 81 (1945).
[3] E. J. Farrell, J. Opt. Soc. Am. **56**, 578 (1966).
[4] T. Orhaug, Optica Acta **16**, 75 (1969).
[5] C. W. Helstrom, J. Opt. Soc. Am. **60**, 233 (1970).
[6] C. W. Helstrom, J. Opt. Soc. Am. **60**, 659 (1970).
[7] J. Zmuidzinas, J. Opt. Soc. Am. A **20**, 218 (2003).
[8] R. Holmes, B. Calef, D. Gerwe, and P. Crabtree, Appl. Opt. **52**, 5235 (2013).
[9] L. Motka, B. Stoklasa, M. D'Angelo, P. Facchi, A. Garuccio, Z. Hradil, S. Pascazio, F. V. Pepe, Y. S. Teo, J. Rehacek, and L. L. Sanchez-Soto, Eur. Phys. J. Plus **131**, 130 (2016).
[10] E. Bettens, D. Van Dyck, A. J. den Dekker, J. Sijbers, and A. van den Bos, Ultramicroscopy **77**, 37 (1999).
[11] S. Ram, E. Sally Ward, and R. J. Ober, P. Natl. Acad. Sci. USA **103**, 4457 (2006).
[12] J. Chao, E. Sally Ward, and R. J. Ober, J. Opt. Soc. Am. A **33**, B36 (2016).
[13] R. A. Fisher, Math. Proc. Cambridge **22**, 700 (1925).
[14] M. Tsang, R. Nair, and X.-M. Lu, Phys. Rev. X **6**, 031033 (2016).
[15] R. Nair and M. Tsang, Phys. Rev. Lett. **117**, 190801 (2016).
[16] R. Nair and M. Tsang, Opt. Express **24**, 3684 (2016).
[17] M. Tsang, New J. Phys. **19**, 023054 (2017).
[18] M. Tsang, J. Mod. Opt. **65**, 104 (2018).
[19] D. Petz and C. Ghinea, "Introduction to Quantum Fisher Information," in *Quantum Probability and Related Topics*, Vol. Volume 27 (World Scientific, 2011) pp. 261–281.
[20] C. Lupo and S. Pirandola, Phys. Rev. Lett. **117**, 190802 (2016).
[21] J. Rehacek, M. Paúr, B. Stoklasa, Z. Hradil, and L. L. Sánchez-Soto, Opt. Lett. **42**, 231 (2017).
[22] M. Paur, B. Stoklasa, Z. Hradil, L. L. Sanchez-Soto, and J. Rehacek, Optica **3**, 1144 (2016).
[23] F. Yang, A. Taschilina, E. S. Moiseev, C. Simon, and A. I. Lvovsky, Optica **3**, 1148 (2016).
[24] F. Yang, R. Nair, M. Tsang, C. Simon, and A. I. Lvovsky, Phys. Rev. A **96**, 063829 (2017).
[25] W. K. Tham, H. Ferretti, and A. M. Steinberg, Phys. Rev. Lett. **118**, 070801 (2017).
[26] C. V. Bennett, R. P. Scott, and B. H. Kolner, Appl. Phys. Lett. **65**, 2513 (1994).
[27] V. Torres-Company, J. Lancis, and P. Andrés, Prog. Opt. **56**, 1 (2011).
[28] R. Salem, M. A. Foster, and A. L. Gaeta, Adv. Opt. Photon. **5**, 274 (2013).
[29] L. Cohen, *Time–Frequency Analysis* (Prentice-Hall, New York, 1995.).
[30] S. Qian and D. Chen, IEEE Signal Process. **16**, 52 (1999).
[31] E. Sejdić, I. Djurović, and J. Jiang, Digit. Signal Process. **19**, 153 (2009).
[32] S. Mallat, *A Wavelet Tour of Signal Processing*, 3rd ed. (Elsevier, New York, 2009).
[33] I. Juvells, A. Carnicer, J. Ferré-Borrull, E. Martín-Badosa, and M. Montes-Usategui, Eur. J. Phys. **27**, 1111 (2006).
[34] B. Lamine, C. Fabre, and N. Treps, Phys. Rev. Lett. **101**, 123601 (2008).
[35] V. Giovannetti, S. Lloyd, and L. Maccone, Nat. Photon. **5**, 222 (2011).
[36] S. Wang, X. Xiang, N. Treps, C. Fabre, R. Dong, T. Liu, and S. Zhang, arXiv:1802.08384 (2018).
[37] A. Lyons, G. C. Knee, E. Bolduc, T. Roger, J. Leach, E. M. Gauger, and D. Faccio, arXiv:1708.08351 (2017).
[38] R. Kaltenbaek, J. Lavoie, D. N. Biggerstaff, and K. J. Resch, Nature Physics **4**, 864 EP (2008).
[39] P. Jian, O. Pinel, C. Fabre, B. Lamine, and N. Treps, Opt. Express **20**, 27133 (2012).
[40] V. Thiel, J. Roslund, P. Jian, C. Fabre, and N. Treps, Q. Sci. Tech. **2**, 034008 (2017).
[41] D. Bradley, B. Liddy, and W. Sleat, Optics Communications **2**, 391 (1971).
[42] J. Rehacek, Z. Hradil, B. Stoklasa, M. Paúr, J. Grover, A. Krzic, and L. L. Sánchez-Soto, Phys. Rev. A **96**, 062107 (2017).
[43] A. Eckstein, B. Brecht, and C. Silberhorn, Opt. Express **19**, 13770 (2011).
[44] P. Manurkar, N. Jain, M. Silver, Y.-P. Huang, C. Langrock, M. M. Fejer, P. Kumar, and G. S. Kanter, Optica **3**, 1300 (2016).
[45] D. V. Reddy and M. G. Raymer, Opt. Express **25**, 12952 (2017).
[46] V. Ansari, G. Harder, M. Allgaier, B. Brecht, and C. Silberhorn, Phys. Rev. A **96**, 063817 (2017).
[47] V. Ansari, J. M. Donohue, B. Brecht, and C. Silberhorn, Optica

5, 534 (2018).
[48] M. Allgaier, V. Ansari, L. Sansoni, C. Eigner, V. Quiring, R. Ricken, G. Harder, B. Brecht, and C. Silberhorn, Nat. Commun. **8**, 14288 (2017).
[49] J. Huang, X. Xie, C. Langrock, R. Roussev, D. Hum, and M. Fejer, Opt. Lett. **31**, 604 (2006).
[50] D. V. Reddy and M. G. Raymer, Optica **5**, 423 (2018).
[51] K. A. G. Fisher, D. G. England, J.-P. W. MacLean, P. J. Bustard, K. J. Resch, and B. J. Sussman, Nat. Commun. **7**, 11200 (2016).
[52] J. H. Munns, S. Park, B. Brecht, and I. A. Walmsley, in *Frontiers in Optics* (Optical Society of America, 2017) pp. JW3A–34.
[53] C. Polycarpou, K. N. Cassemiro, G. Venturi, A. Zavatta, and M. Bellini, Phys. Rev. Lett. **109**, 053602 (2012).
[54] J. Roslund, R. M. De Araujo, S. Jiang, C. Fabre, and N. Treps, Nat. Photonics **8**, 109 (2014).